Proceedings of the 21st ICSMGE, Vienna, Austria, 14 – 19 June 2026. Pistrol, Adam & Schweiger (eds.)
Published by: ÖGG, Austrian Society for Geomechanics, Salzburg, Austria, ISBN 978-3-9503898-4-5
https://doi.org/10.53243/ICSMGE2026-2361

Inverse analysis of density using muography with Lasso regression

Toshifumi Shibata, Shin-ichi Nishimura
Okayama University, Okayama, Japan, tshibata@cc.okayama-u.ac.jp

ABSTRACT: The paper describes a newly developed cross-hole muography technique for measuring ground density by installing small-size muon detectors in boreholes. Muography measurement results are analyzed for their statistical characteristics and are used to propose a method for evaluating ground density through short-duration measurements with Lasso regression, along with an examination of its accuracy. First, model tests on a soil layer are conducted to obtain the statistical distribution of daily muon measurement data. Subsequently, muography is carried out by installing detectors in boreholes within an embankment, and the statistical characteristics were derived from the measurement results. Then, to establish a method for detecting low-density regions—i.e., weak zones in the ground—in a virtual geo-structure, numerical analysis using Lasso regression was performed based on the muography results. Finally, the applicability of muography to site investigations of geo-structures is discussed.

KEYWORDS: Lasso regression, muography, ground density.

1 INTRODUCTION

In recent years, heavy rainfall disasters have been increasing due to climate change, and there is a high probability that large-scale earthquakes, such as a Nankai trough earthquake, will occur, raising concerns about damage to infrastructures. Many infrastructures have been in use for a long time, making proper maintenance and management increasingly important. To inspect and maintain infrastructures, such as soil structures, it is essential to evaluate their condition through subsurface exploration. However, conventional methods of diagnosis have been unable to simultaneously satisfy both exploration depth and resolution. Conducting investigations using cosmic-ray muons, namely, muography, is expected to be a promising method for solving these challenges in subsurface investigations.

Muography has been applied in various fields up to the present. In 1955, George attempted to estimate the density of rocks within a mine, and in 1970, Alvarez et al. conducted muon measurements on a pyramid. Later, Morishima et al. (2017) discovered a cavity in the Great Pyramid of Khufu. Suzuki (2012) measured the positions of the passage and a sewage pipe, and Tanaka et al. (2014) investigated magma dynamics at the Satsuma Iwojima volcano, and Tanaka *et al*. (2022) expanded the application of muography to atmospheric phenomena. Additionally, Namikawa et al. (2024) applied muography to visualize the internal structure of river embankments.

A cosmic-ray muon is a type of elementary particle. Cosmic rays are classified into primary and secondary cosmic rays. The former rays enter the Earth directly, while the latter ones are produced when the primary cosmic rays collide and interact with atomic nuclei in the Earth's atmosphere. About 70% of secondary cosmic rays consist of muons, and these muons have excellent penetration capability due to their extremely small size. However, as the distance and density of the material through which they pass increase, muons lose energy and are more likely to decay into electrons and neutrinos. Therefore, as the product of the average density and the vertical distance increases, muons lose more energy while passing through the material, resulting in a decrease in the number of muons that penetrate it. Using this property, the average density of a material can be estimated based on the number of detected muons. Although this is a relatively simple method, achieving both high accuracy and a short measurement time in muography is challenging and usually requires long-duration measurements.

This paper presents newly developed cross-hole muography, taking measurements through the installation of small-size muon detectors in boreholes. A method to obtain ground density within short measurement times, based on measurements of muography using Lasso regression, is presented, and its accuracy is verified. Firstly, model tests on a soil layer are carried out to verify the muon measurement status per day. Secondly, muography is conducted on earth-fill. Subsequently, a numerical analysis to confirm the possibility that muography can detect low-density regions, namely, weak areas, is conducted for the virtual geo-structure based on the statistical properties obtained from the conducted experiments. Lasso regression is employed as an inverse analysis method. Finally, the applicability of muography to site investigations of geo-structures is discussed.

2 CROSS-HOLE MUOGRAPHY

2.1 *Model tests on soil layer*

Muons are measured with the small-size muon detector shown in Figure 1 (a), (b), which consists of a spherical plastic scintillator and a photomultiplier tube. Due to its small size, the detector can be installed in a borehole.

(a) Photo of detector.

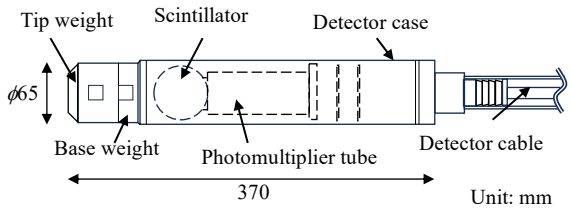

(b) Schematic of detector.

Figure 1. Small-size muon detector.

In addition, a weight is attached to this detector to prevent it from floating when installed below the groundwater level. Two of these detectors are connected to the measurement unit and the computer via cables. The transmission of muons through

each scintillator is extracted as faint light, converted into electrical signals in the photomultiplier, and then recorded as counts. The arrival direction of the muons can be determined by detecting the muons that have passed through both scintillators. The muon counts per unit time, unit area, and unit solid angle, that travel through the two detectors simultaneously, are measured. The counts of electrical signals are saved as a digital file in the computer. As shown in Figure 2, one detector is installed on each side of a soil layer, which has a height of 200 cm and a width of 55 cm, in order to check the measurement status of the muons. Furthermore, measurements are also conducted with only the two detectors installed at a width of 85 cm, without the soil layer situated between them. This arrangement assumes the installation of the detectors in two boreholes and is referred to as cross-hole muography. Figure 3 shows the distribution of muon

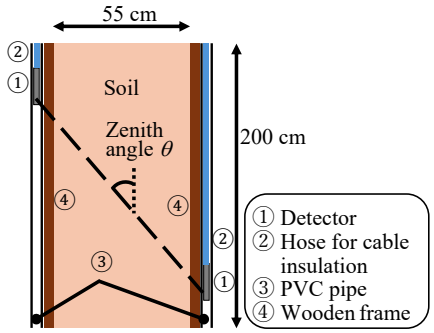

Figure 2. Small-size muon detector.

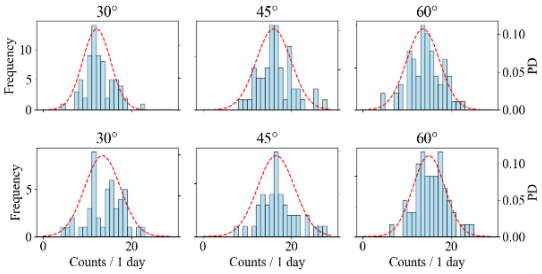

Figure 3. Distribution of counts of muon.

counts per day. The upper row in the figure indicates the measurement results for the soil layer, while the lower row indicates the results with no soil structure. From left to right, the results are shown for zenith angles of 30°, 45°, and 60°, respectively. Figure 3 shows that the number of muon counts over a fixed period follows a normal distribution.

2.2 *Field experiment on earth-fill*

Figure 4 shows a diagram of the earth-fill with two boreholes for the muon measurements. Two scintillators are installed in the two boreholes (A) and (B) in the embankment, respectively. Figure 5 shows the positions of the detectors, with the detector in borehole (A) installed at a deeper location.

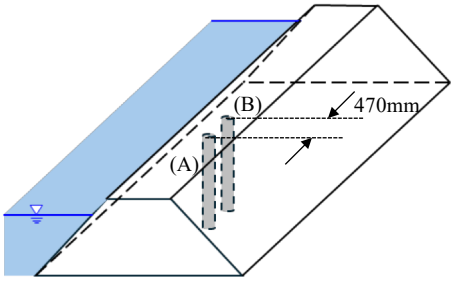

Figure 4. Schematic diagram of earth-fill with two boreholes.

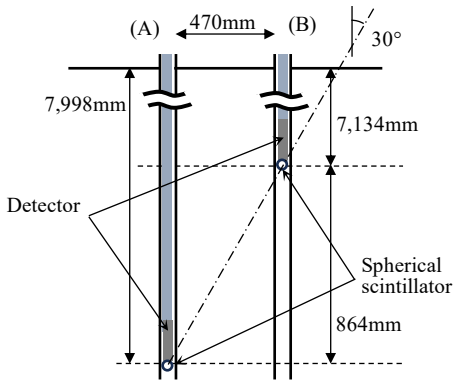

Figure 5. Positions of the two scintillators in boreholes.

Using the measurement system described in the previous section, the number of muons passing from the ground surface through the embankment is counted and, from the results, the density of the embankment material is calculated. The flux, i.e., the muon counts per unit time, unit area, and unit solid angle, that simultaneously pass through the detectors, is measured, and the mean density, multiplied by the vertical distance obtained by Minato's formula (Minato, 1992), is determined by Eqs. (1), (2), and (3).

$$I = I_0 \cos^n \theta \exp\left(-\frac{h}{\Lambda(h)}\right) \tag{1}$$

$$\Lambda(h) = A + Bh + Ch^2 \tag{2}$$

$$n = \alpha + \beta h \tag{3}$$

where I is the flux, h is the mean density multiplied by the vertical distance, θ is the zenith angle, and I_0, A, B, C, α, and β are parameters with I_0=0.00723 (/cm^2/s/sr), A=17.61 (cm^2/hg), B=0.1404 (cm^4/hg^2), C=-7.069×10^{-5}(cm^6/hg^4), α=1.495, and β=0.02018(cm^2/hg); these values were obtained from experiments in previous study. The unit sr represents the unit solid angle. I and the muon count are calculated from Eq. (1), and the density is determined from the vertical distance and h.

The density of the embankment soil, obtained from the samples during the borehole drilling, was taken as the test value, which is conventionally called the "pre-test density", while the density calculated from the muon count measurements is taken as the measured value, which is conventionally called the "measured density". The pre-test density is 1.95 (g/cm^3) and the measured density is 2.20 (g/cm^3), showing a difference of 0.25 (g/cm^3).

Subsequently, the statistical properties are examined. The muon generation phenomenon is a random process based on a Poisson process, and the number of occurrences follows a Poisson distribution within a fixed time and space. When the number of observations is large, the Poisson distribution can be approximated by a normal distribution. The normality is verified by the model tests depicted in Figure 3. Therefore, the statistical properties based on the normal distribution using experimental data are verified. The relationship between the number of counts and the variance in muon measurements is also examined. It is also known that, in radiation measurements, the relationship between count number N and standard deviation σ is given by Eq. (4).

$$\sigma = \sqrt{N} \tag{4}$$

Table 1 shows the mean (Mean) calculated from the measurement results for one and two days, the standard

deviation (SD), and the standard deviation (SD-eq) calculated from Eq. (1). From the table, it is seen that the measured results are close to the values obtained from Eq. (1), demonstrating that Eq. (1) is also applicable for muon measurements.

Table 1. Mean and standard deviations.

	1 day	2 days
Mean (g/cm^3)	7.31	14.66
SD (g/cm^3)	2.54	3.40
SD-eq (g/cm^3)	2.70	3.83

3 NUMERICAL ANALYSIS

This chapter presents a simulation of muon measurements using a two-dimensional numerical analysis model, followed by an analysis of the results using Lasso regression.

3.1 *Lasso regression*

Lasso regression (Tibshirani (1996)) is a linear regression method expressed as the minimization problem shown by Eq. (5).

$$\min_{x}\left(\frac{1}{2\lambda}\|\boldsymbol{y}-\boldsymbol{A}\boldsymbol{x}\|_2^2+\|\boldsymbol{x}-\boldsymbol{x}_0\|_1\right) \tag{5}$$

where $\boldsymbol{y}$ represents the observed vector, $\boldsymbol{x}$ denotes the vector of unknown parameters, $\boldsymbol{x}_0$ is the prior information on $\boldsymbol{x}$, $\boldsymbol{A}$ is a linear operator, and λ is the Lagrange multiplier. Eq. (5) consists of a least squares term and a regularization term. The least squares term represents the sum of the squared residuals between the predicted and the observed values, while the regularization term is the L_1 norm, which represents the sum of the absolute values of each component. As a method for solving the L_1 norm minimization problem, the Alternating Direction Method of Multipliers is employed (Boyd *et al*. (2010)), and λ is determined by the L-curve method (Hansen (1992)). This paper defines $\boldsymbol{y}$ as the product of the average density and the vertical distance, $\boldsymbol{A}$ as the distance of the measuring line for each element, $\boldsymbol{x}$ as the density of each element, and $\boldsymbol{x}_0$ as the prior information on the density.

3.2 *Numerical model of ground*

Figure 6 shows the two-dimensional model with a low-density region, measuring points, and measuring lines. The mesh size of the ground is 0.5 m × 0.5 m, and the diameter of the four boreholes is 70 mm, while the scintillators inside the detectors have a diameter of 51 mm. Additionally, the low-density region is a square, with dimensions of 1 m × 1 m, that is positioned at a depth of 4 m from the ground surface. The ground density is set to 2.0 g/cm^3, and the density of the low-density region in the ground is set to 0.0 g/cm^3.

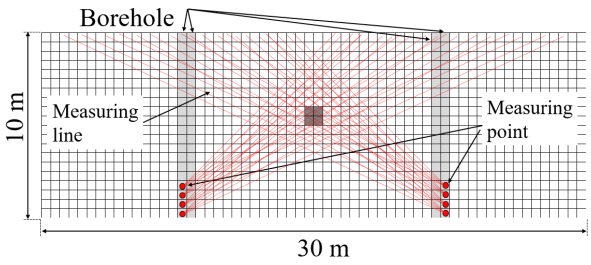

Figure 6. Schematic diagram of ground model, measuring points, and measuring lines.

3.3 *Muon simulation method*

The muon measurement count is simulated by the Monte Carlo method, and the results are estimated using Lasso regression. When using the Monte Carlo method, temporal and spatial variations during the muon measurement process are considered. This paper generates random numbers based on the angles of incidence at the positions of the two detectors, reflecting the spatial variations in Figure 7. Next, for each angle of incidence, random numbers are generated based on a normal distribution reflecting the temporal variations, as described in section 2.2. Then, the product of the average density and the vertical distance along the measuring line is obtained according to the measurement counts. The density of each element is computed through Lasso regression using that value.

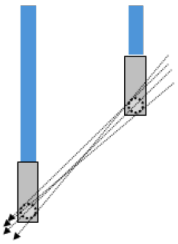

Figure 7. Spatial variations.

The entire process, from simulating the muon measurement count to analyzing it using Lasso regression, is repeated 1,000 times. For each element of the analysis model, the mean ground density, standard deviation of the density, and probability of falling below the initially set ground density are calculated. By setting the initial value of the regularization term to a ground density of 2.0, this term converges to 2.0, while simultaneously approaching the density of the analysis model. This helps suppress measurement errors and makes it possible to shorten the measurement time.

The conditions for the numerical analysis are set as follows: the number of measurement points is four, and the measurement angles are 45, 50, 55, 60, and 65 degrees. Two cases are considered for the low-density region: 0.0 g/cm^3 and 1.0 g/cm^3. Here, the results of the numerical analysis shown later are presented only for the case with a density of 0.0 g/cm^3. For each of these cases, three different average count numbers are examined: 25, 50, and 100, resulting in a total of six cases. It should be noted that the numbers of measurement points and measurement angles are based on one borehole, whereas an actual numerical analysis is conducted using two boreholes, namely, one on each side.

4 RESULTS

Figure 8 (a), (b), and (c) display the average density, probability of falling below a density of 2.0 g/cm^3, and standard deviation when the low-density region has a density of 0.0 g/cm^3 and the average count is 25. The average density of the low-density region is calculated to be lower than that of the surrounding area, suggesting that the low-density region is identifiable. The density of this region is 1.940 g/cm^3, and the difference in density between the low-density region and the surrounding area is clear. From Figure 8 (b), it is seen that, in the low-density region, the probability of falling below the ground model density is higher compared to the surrounding area. The low-density region is recognized since the probability is 0.649. At this point, the measurement time was up to three days per measurement angle. Figure 8 (c) shows that the standard deviation is low in the center of the ground model. This is because the measurement ranges overlap, resulting in more measurement data for the corresponding area. Figure 8 (d), (e)

and (f) present the distribution of the average density, the probability of falling below the ground model density, and standard deviation when the average count is 50.

From Figure 8 (d) and (e), it can be seen that the low-density region is more clearly defined compared to the case

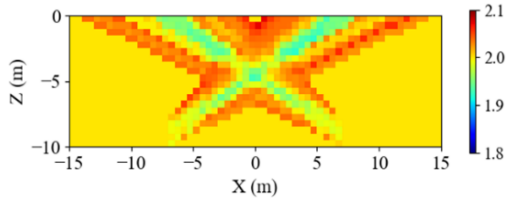

(a) Average density with average count of 25.

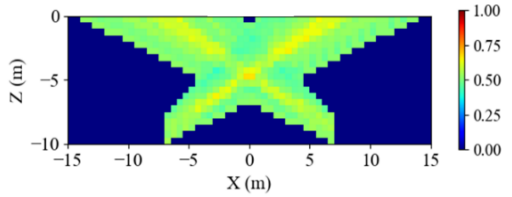

(b) Probability of density falling below 2.0 g/cm^3 in low density region with average count of 25.

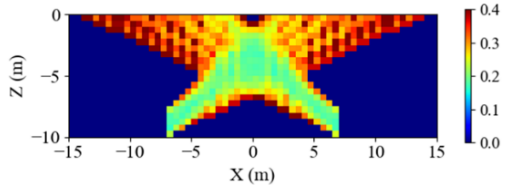

(c) Standard deviation of density with average count of 25.

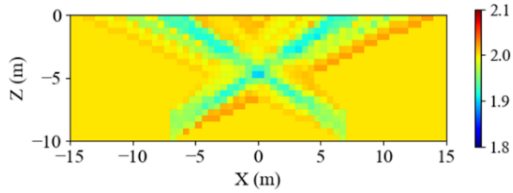

(d) Average density with average count of 50.

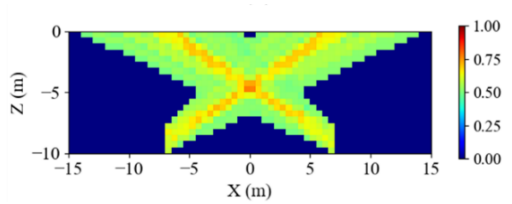

(e) Probability of density falling below 2.0 g/cm^3 in low density region with average count of 50.

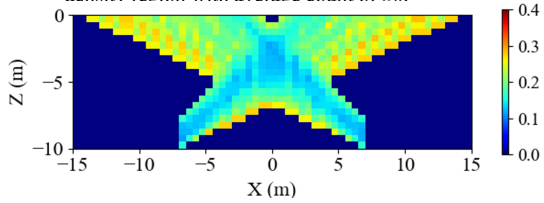

(f) Standard deviation of density with average count of 50.

Figure 8. Mesh map of numerical results.

with an average count of 25. The average density of the low-density region is 1.914 g/cm^3 and the probability is 0.752, indicating an improvement in accuracy in the numerical results. Figure 8 (f) also shows that the standard deviation is low at the center of the ground model. In this case, the measurement time was up to six days per measurement angle.

5 CONCLUSIONS

The applicability of the ground density identification method by the newly proposed cross-hole muography has been presented for geo-structures. In the method, Lasso regression was employed and found to work well as an inversion method using the statistical characteristics of daily muon measurement data. This study has demonstrated that a probabilistic evaluation of ground density is sufficiently feasible even with a measurement period of approximately three days, although it is evident that extending the measurement period to increase the number of detected muons allows for a more accurate estimation of density.

6 ACKNOWLEDGEMENTS

This work was partly supported by JSPS KAKENHI Grant Numbers 20H00442 and 24H00534. The valuable suggestions and comments by Dr. Keiichi Suzuki of the Fukada Geological Institute are gratefully acknowledged. The authors greatly appreciate the contribution of Mr. Ken Takahashi to this research project.

7 REFERENCES

Alvarez, L.W., Anderson, J.A., EI Bedwei, F., Burkhard, J., Fakhry, A., Girgis, A., Goneid, A., Hassan, F., Iverson, D., Lynch, G., Miligy, Z., Moussa, A.H., Sharkawi, M., and Yazolino, L. 1970. Search for Hidden Chambers in the Pyramids. Science, 167, 832-839. https://www.science.org/doi/10.1126/science.167.3919.832.

Boyd, S., Parikh, N., Chu, E., Peleato, B., and Eckstein, J. 2010. Distributed Optimization and Statistical Learning via the Alternating Direction Method of Multipliers. Foundations and Trends in Machine Learning, 3(1), 1–122.

George, E.P. 1955. Cosmic rays measure overburden of tunnel. Commonwealth Engineer, 42(12), 455-457.

Hansen, P.C. 1992. Analysis of Discrete Ill-Posed Problems by Means of the L-Curve, SIAM Review, 34(4), 561-580.

Minato, S. 1992. Cosmic-Ray Transmitted Images. Radiation, 19(1), 49-56. (in Japanese)

Morishima, K., Kuno, M., Nishio, A., Kitagawa, N. Namabe, Y., Moto, M., Takasaki, F., Fujii, H., Satoh, K., Kodama, H., Hayashi, K., Odaka, S., Procureur, S., Attié, D., Bouteille, S., Clavet, D., Filosa, C., Magnier, P., Mandjavidze, I., Riallot, M., Marini, B., Gable, P., Date, Y., Sugiura, M., Elshayeb, Y., Elnady, T., Ezzy, M., Guerriero, E., Steiger, V., Serikoff, N., Mouret, J.B., Cjarlés, B., Helal, H., and Tayoubi, M. 2017. Discovery of a big void in Khufu's Pyramid by Observation of Cosmic-ray Muons. Nature, 552, 386-390, 10.1038/nature24647.

Namikawa, K., Koyama, N., Kusagaya, T., Suzuki, K., Yamada, T., and Yamada, T. 2024. New cosmic ray muon tomography for visualizing internal of river embankment. Japanese Journal of JSCE, 80(16), 23-16156. (in Japanese)

Suzuki, K. 2012. Feasibility study of geophysical exploration for civil engineering using cosmic ray muons. Exploration Geophysics, 65(4), 251-259. (in Japanese)

Tanaka, H.K.M., Kasugaya, T., and Shinohara, H. 2014. Radiographic visualization of magma dynamics in an erupting volcano. Nature communications, 10.1038/ncomms4381.

Tanaka, H.K.M., Gluyas, J., Holma, M., Joutsenvaara, J., Kuusiniemi, P., Leone, G., Presti, D.L., Matsushima, J., Oláh, L., Steigerwald, S., Thompson, L.F., Usoskin, I., Poluianov, S., Varga, D., and Yokota, Y. 2022. Atmospheric Muography for Imaging and Monitoring Tropic Cyclones. Scientific Reports, 12.https://www.nature.com/articles/s41598-022-20039-4

Tibshirani, R. 1996. Regression shrinkage and selection via the lasso, Journal of the Royal Statistical Society. Series B (Methodological), 58(1), 267-288.